Neuron
Article

Photoreceptor-Derived Activin Promotes Dendritic Termination and Restricts the Receptive Fields of First-Order Interneurons in *Drosophila*

Chun-Yuan Ting,[1,6] Philip G. McQueen,[2,6] Nishith Pandya,[3] Tzu-Yang Lin,[1] Meiluen Yang,[1] O. Venkateswara Reddy,[4] Michael B. O'Connor,[5] Matthew McAuliffe,[3] and Chi-Hon Lee[1,*]
[1]Section on Neuronal Connectivity, Laboratory of Gene Regulation and Development, Eunice Kennedy Shriver National Institute of Child Health and Human Development
[2]Mathematical and Statistical Computing Laboratory, Division of Computational Bioscience, Center for Information Technology
[3]Biomedical Imaging Research Services Section, Center for Information Technology
National Institutes of Health, Bethesda, MD 20892, USA
[4]National Center for Biological Sciences, Tata Institute of Fundamental Research, GKVK Campus, Bangalore 560065, India
[5]Department of Genetics, Cell Biology and Development, University of Minnesota, Minneapolis, MN 55455, USA
[6]These authors contributed equally to this work
*Correspondence: leechih@mail.nih.gov
http://dx.doi.org/10.1016/j.neuron.2013.12.012

SUMMARY

How neurons form appropriately sized dendritic fields to encounter their presynaptic partners is poorly understood. The *Drosophila* medulla is organized in layers and columns and innervated by medulla neuron dendrites and photoreceptor axons. Here, we show that three types of medulla projection (Tm) neurons extend their dendrites in stereotyped directions and to distinct layers within a single column for processing retinotopic information. In contrast, the Dm8 amacrine neurons form a wide dendritic field to receive ~16 R7 photoreceptor inputs. R7- and R8-derived Activin selectively restricts the dendritic fields of their respective postsynaptic partners, Dm8 and Tm20, to the size appropriate for their functions. Canonical Activin signaling promotes dendritic termination without affecting dendritic routing direction or layer. Tm20 neurons lacking Activin signaling expanded their dendritic fields and aberrantly synapsed with neighboring photoreceptors. We suggest that afferent-derived Activin regulates the dendritic field size of their postsynaptic partners to ensure appropriate synaptic partnership.

INTRODUCTION

Dendrites adapt stereotyped branched morphologies that correlate with their neuronal identity. The type-specific dendritic organization is a key determinant of synaptic connectivity and the neural computation subserved by the dendrites (reviewed in London and Häusser, 2005). Theoretical analyses show that the dendrites of pyramidal and Purkinje cells are organized to maximize the connectivity repertoire at a given wiring cost and that their drastically different dendritic morphologies are the optimized solutions for the distinct arrangements of their presynaptic partners (Wen et al., 2009). In the vertebrate retina, about 20 types of retinal ganglion cells and 30 types of amacrine neurons have been identified based on morphologies: i.e., their dendritic field size, branching complexity, and layer-specific arborizations (Masland, 2012; Völgyi et al., 2009). These dendritic properties determine the neurons' functional receptive field and, thus, the sampling and processing of visual signals in the field.

Recent genetic studies, especially of the dendritic arborization (da) sensory neurons in the fly peripheral nervous system and of neurons in the mouse retina, have begun to unravel the mechanisms of dendritic morphogenesis and routing. These studies have shown that intrinsic mechanisms, such as cell-type-specific or graded expression of transcription factors, regulate overall dendrite morphogenesis (reviewed in Jan and Jan, 2010). Extracellular cues, such as the Semaphorins, have been shown to direct layer-specific dendritic arborization (Matsuoka et al., 2011). The homophilic immunoglobulin superfamily proteins, such as Sidekicks, are expressed in distinct subsets of retinal neurons to promote layer-specific arborization of dendrites and synapse formation with the interneurons expressing the same family members (Yamagata and Sanes, 2008).

Much less is known about how dendritic field size is regulated. In the *Drosophila* da neurons, the Down syndrome cell adhesion molecule (DSCAM) provides a mechanism to avoid overlapping of dendrites from the same neurons (self-avoidance) and neighboring neurons of the same type (tiling), via stochastic expression of splice variants that afford homotypic repulsive activity (Matthews et al., 2007). Protocadherin Pcdhg isoforms carry out functions analogous to those of DSCAM in cerebellar Purkinje cells and the starburst amacrine neurons of the mouse retina (Lefebvre et al., 2012). As mutual repulsion is most effective for tiling dendrites when the dendrites are confined to a two-dimensional space (Han et al., 2012), additional mechanisms likely exist to regulate the dendritic field size and to match with presynaptic partners in three-dimensional (3D) space, such as in the mammalian cortex.

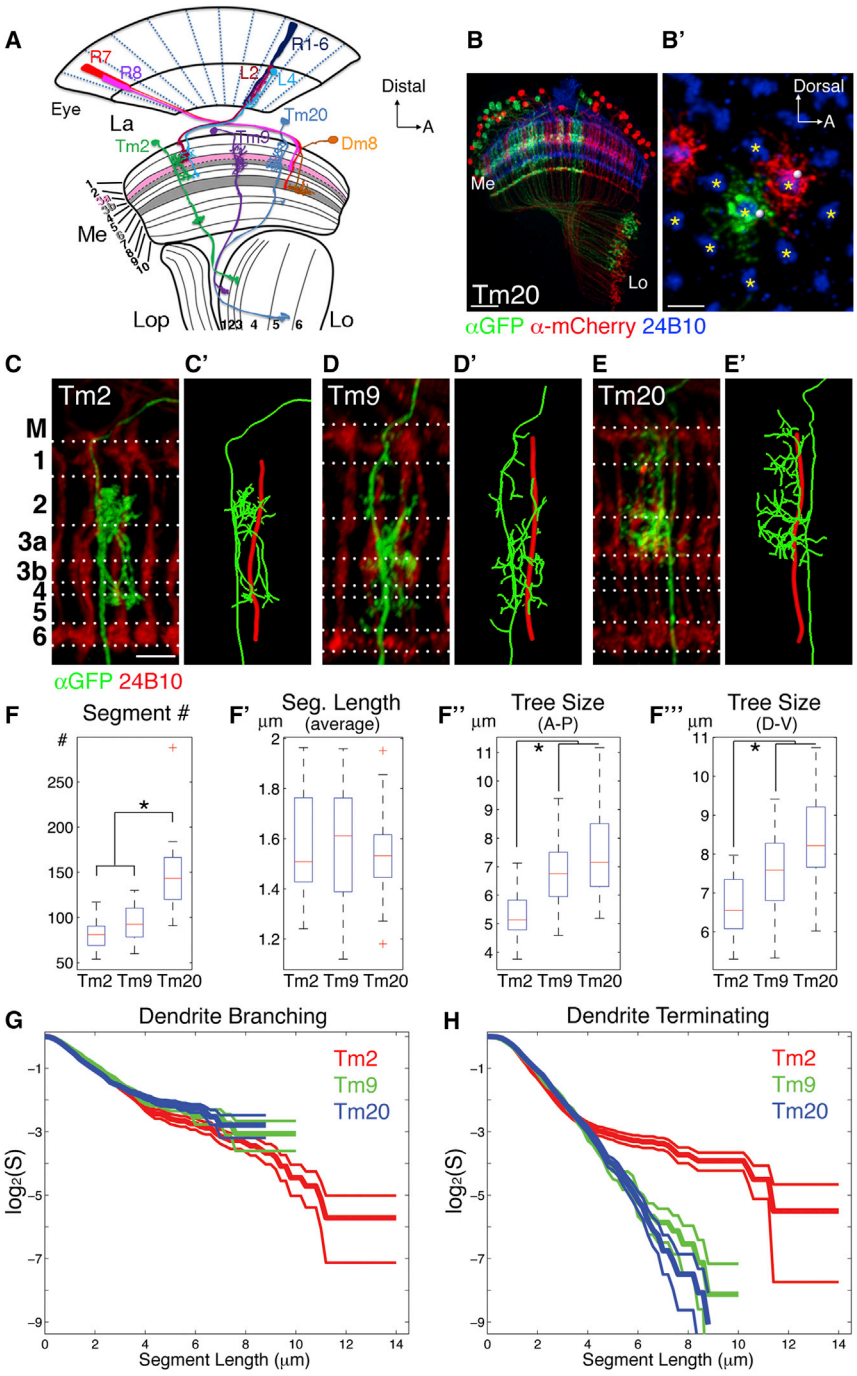

Figure 1. Dendritic Morphologies and Branching and Terminating Frequencies of Three Types of Medulla Projection Neurons, Tm2, Tm9, and Tm20

(A) A schematic illustration of the *Drosophila* visual system, including the eye (Eye), and four optic neuropils: lamina (La), medulla (Me), lobula (Lo), and lobula plate (Lop). Three types of transmedulla (Tm) neurons and one type of distal medulla (Dm) neurons are shown. Tm2 (green), Tm9 (purple), and Tm20 (light blue) extend their dendrites at different medulla layers to receive inputs from their synaptic partners, L2/4, L3, and R8 (magenta), respectively; they project their axons to distinct lobula layers (Lo2, Lo1, and Lo5, respectively). The wide-field Dm8 amacrine neurons (orange) extend their dendrites in layer M6 to receive inputs from R7 (red). Distal and anterior (A) orientations are with respect to the head.

(B and B′) Tm20 dendrites clustered in single columns and show limited overlapping with neighboring Tm20 dendrites. Tm20 neurons were labeled stochastically by mCD8-GFP (green) and rCD2-mCherry (red) and were visualized with anti-GFP and anti-mCherry antibodies at the adult stage. Axonal positions of two adjacent Tm20 are marked with spheres. Photoreceptor axons were visualized with the 24B10 antibody (blue) and are marked with asterisks. (B) and (B′) show dorsal-ventral and proximal-distal views, respectively. Dorsal and anterior (A) directions are as indicated. Scale bars, 20 μm in (B) and 4 μm in (B′).

(C–E′) The dendritic morphologies of three Tm neurons, Tm2 in (C) and (C′), Tm9 in (D) and (D′), and Tm20 in (E) and (E′), were revealed by the dual-view imaging technique. Single Tm neurons were stochastically labeled with the mCD8GFP marker (green), using cell-specific-Gal4 drivers. Photoreceptor axons were visualized with the 24B10 antibody (red). Confocal images collected in two orthogonal directions were deconvolved and combined to form 3D stacks, and the neurites were traced as shown in (C′), (D′), and (E′). The photoreceptor axons in the cognate column are shown as red filaments. Scale bar, 5 μm.

(F–F‴) Box plots show four metrics for the dendritic trees of wild-type Tm2, Tm9, and Tm20 neurons. Tm20 neurons have more dendritic segments (segment #, in F) than Tm2 and Tm9 do. The averaged lengths of dendritic segments (segment length average, in F′) for the three wild-type Tm neurons are not significantly different. Tm20 and Tm9 have larger dendritic trees than Tm2 neurons do, as shown in (F″) and (F‴). *$p < 0.05$, Wilcoxon rank-sum test with Bonferroni correction.

(G and H) Kaplan-Meier estimates (S, y axis) of (G) dendrite branching and (H) dendrite terminating were plotted in logarithmic scale base 2, with respect to segment length (x axis). Thick and thin lines denote averages ± SDs. Tm2 (red), Tm9 (green), and Tm20 (blue) shared similar dendrite branching and terminating frequencies for segments less than 4 μm.

To study dendritic development further, we chose to use the *Drosophila* visual system, which is an excellent model for studying axon guidance (Sanes and Zipursky, 2010; Melnattur and Lee, 2011). The medulla, the largest neuropil of the optic lobe, is organized in layers (M1–M10) and columns (Figure 1A; Fischbach and Dittrich, 1989), in a fashion reminiscent of the mammalian visual cortex. All visual information received by photoreceptors converges to the distal medulla (M1–M6): the axons of narrow-spectrum R7 and R8 photoreceptors directly innervate the M6 and M3 layers, respectively, while the lamina neuron

L1–L3 relay information from the broad-spectrum R1–R6 photoreceptors to multiple medulla layers. The terminals of the R7, R8, and L1–L3 neurons that view a single point in visual space innervate a single medulla column (Takemura et al., 2008), thereby establishing a retinotopic pixel. Thus, the medulla columns directly correspond to a functional visual field, an attribute greatly facilitating structure-function studies.

The medulla contains over 60 morphologically distinct types of neurons, each of which arborizes dendrites in different medulla layers and has a characteristic receptive field size (Fischbach and Dittrich, 1989). The projection neurons (called transmedulla [Tm] neurons) project their axons to a higher visual center, the lobula complex, while the intrinsic neurons, such as the wide-field amacrine (Dm) neurons, provide interconnections among columns and/or layers (Figure 1A). The presynaptic partners of medulla neurons and their visual functions have been studied extensively (Takemura et al., 2013). Tm2 neurons relay motion-detection inputs from L2 and L4 neurons to the lobula (Takemura et al., 2011), while Tm9 and Tm20 neurons relay chromatic information from L3 and R8 to distinct lobula layers (Gao et al., 2008; Karuppudurai and C.-H.L., unpublished data). The wide-field Dm8 amacrine neurons pool inputs from about 16 UV-sensing R7 photoreceptors and relay the information to the Tm5c neurons, thereby enhancing UV sensitivity (Gao et al., 2008; Karuppudurai and C.-H.L., unpublished data). While considerable progress has been made in understanding how axons of photoreceptors and lamina neurons target different medulla layers and their retinotopically appropriate columns, essentially nothing is known about how the medulla neurons route their dendrites to meet their appropriate presynaptic partners.

In this study, we investigated the routing of dendrites of medulla neurons in 3D space. Using a dual-view imaging technique, we reconstructed the dendritic arbors of three types of Tm neurons: Tm2, Tm9, and Tm20. By registering dendritic traces against a reference array of medulla columns, we identified type-specific dendritic attributes. We further identified that Activin signaling regulates a specific aspect of dendritic patterning in the projection neuron Tm20 and the wide-field amacrine neuron Dm8. We showed that Activin derived from R7 and R8 photoreceptors acts instructively on their respective target neurons, Dm8 and Tm20, to restrict their dendritic field to the size appropriate for the neurons' functions.

RESULTS

Dual-View Imaging Reveals the Dendritic Morphologies of Three Types of Transmedulla Neurons in 3D Space

To identify cell-type-specific drivers for labeling Tm2, Tm9, and Tm20 neurons, we screened a collection of promoter-Gal4 lines and further refined their expression patterns using the Split-Gal4 system (Figure S1 available online; for details, see Supplemental Experimental Procedures; Luan et al., 2006). Using a flip-out genetic mosaic method (Wong et al., 2002), we imaged single Tm2, Tm9, and Tm20 neurons and confirmed their cell identities by their stereotypic dendritic morphologies in the medulla (Figures 1C–1E′) and layer-specific termination of axons in the lobula (data not shown), as described in a previous Golgi study (Fischbach and Dittrich, 1989). The three Tm neurons were present in most, if not all, columns and were therefore likely to be invariant components of the columns. We further examined the dendritic arbors of neurons of the same type in neighboring columns by stochastically labeling neurons with GFP and mCherry (see Experimental Procedures for details). This double-stochastic labeling experiment revealed that the dendrites of individual neurons cluster around a single pair of R7 and R8 photoreceptor axons and show minor overlap with the dendrites of neighboring neurons (Figure 1B′). These anatomical findings are consistent with the idea that these neurons primarily process retinotopic information within single medulla columns (Figures 1C–1E′) and relay the information to distinct layers in a higher visual center, the lobula (Figure 1A).

Analyzing dendritic morphologies of Tm neurons requires imaging and tracing their complex dendritic arbors in three dimensions; this is technically challenging with conventional confocal microscopy, which has a low axial resolution (Fischer et al., 2011). We therefore developed a dual-view imaging procedure that uses image deconvolution and combination methods to mitigate the axial distortion problem (Figure S2). Confocal image stacks of single neurons were collected from two orthogonal directions, deconvolved, and then fused using a custom software package to generate 3D images (Figure S2; see Experimental Procedures for details). While the image resolution is limited by diffraction, which precludes the measurement of dendritic calibers and of fine dendritic spikes (<0.2 μm), the resulting images allowed reliable tracing of most dendritic arbors in 3D (Figures S2D–S2E″ and S3A–S3C).

Morphometric Analyses Reveals Differences in Dendrite Branch Numbers and Tree Sizes

Using a semiautomatic tracing program, we constructed about 20 skeletonized dendritic trees for each neuronal type. Visual inspection revealed that these dendritic traces recapitulated previously described morphological features (Figures 1C–1E′). However, the detailed branching patterns varied greatly among neurons of the same type (Figures S3A–S3C). To characterize the dendritic patterns of Tm neurons, we calculated a set of standard dendritic metrics using L-measure, a neuromorphometric analysis program (Scorcioni et al., 2008). The metrics obtained provided limited statistical power to differentiate among these three neuronal types. Tm20 neurons have, on average, more dendritic segments than Tm2 and Tm9 neurons (Figure 1F), which in part reflected the Tm20s' larger dendritic trees (Figures 1F″–1F‴). The other metrics, including average segment length, local branching geometry, and global contraction and symmetry, were comparable among the three types (Figures 1F′ and S3H–S3O). We further analyzed the branching and terminating frequencies based on a Kaplan-Meier nonparametric estimator (KME; Kaplan and Meier, 1958; see Experimental Procedures for details). The KME curves revealed that the logarithm of the KME for branching and terminating was inversely correlated with the branch lengths for all three Tm neuron types (Figures 1G and 1H). Thus, the branching and terminating frequencies (as estimated by the first derivative of the KME curve) appeared to be largely independent of the segment length. An exception was a reduced termination frequency for the longer segments (>4 μm) of Tm2, which was attributed to the long dendritic legs

that terminate in the M4–M5 layers. For dendritic segments of ~0.5 to ~4 μm, the branching/terminating frequencies for the three types were similar: Tm2, 0.393/0.602; Tm9, 0.371/0.589; and Tm20, 0.360/0.594 events per micrometer.

Registration to Reference Columns Reveals Type-Specific Dendritic Attributes

Because typical morphometric analyses failed to differentiate reliably among the dendritic patterns of the three Tm types, we reasoned that the spatial relationship between the dendritic trees and the medulla columns they reside in could contribute to the type-specific dendritic attributes. To account for sample variations in size and orientation, we developed a landmark-based registration method to standardize the dendritic patterns. First, we modeled nine medulla columns as a rhombic array based on the measurements of about 120 columns (Figures 2B and S4A–S4E′) and stratified the distal medulla into seven layers based on the terminals of L1, L2, L3, R8, and R7, as well as on the anti-Connectin staining pattern (Figures S4F–S4J; Fischbach and Dittrich, 1989). Second, we developed an automatic registration method that used photoreceptor axons as landmarks to carry out affine and nonlinear registration of dendritic trees to the reference column array (Figures 2B and 2C; see Supplemental Experimental Procedures for details).

The registration of dendritic trees to the reference columns revealed that different Tm neurons preferentially projected dendrites to distinct medulla layers (Figures 3A–3B″), a feature that has been used to differentiate medulla neuron types previously (Fischbach and Dittrich, 1989). The layer matching of medulla dendritic terminals with afferent terminals at least in part reflects their connectivity with a few predominant presynaptic partners (for example, L2 and L4 for Tm2). A pairwise comparison of dendritic traces of the same and different neuronal types revealed that layer-specific termination of dendrites was a strong metric for accurately classifying these Tm neurons (Figure S5A).

Most important, examining the registered dendritic trees revealed a number of dendritic attributes that eluded previous analyses. First, with respect to their cognate column, the axons of different Tm types are segregated along the posterior-anterior axis: Tm2 and Tm9 axons extended along the posterior edge of the column, and Tm20 axons extended at the anterior edge (Figure 2C′; SDs were 0.46 μm for Tm2, 0.63 μm for Tm9, and 0.62 μm for Tm20 at the M3a/M3b boundary). In contrast, the axonal positions along the dorsal-ventral axis were highly variable (SDs were 1.08 μm for Tm2, 1.18 μm for Tm9, and 2.18 μm for Tm20 at the M3a/M3b boundary). Second, dendrites extended from the axons to innervate their cognate columns in preferred planar orientations: Tm20 dendrites projected posteriorly, and Tm2 and Tm9 dendrites projected anteriorly (Figures 3C–3D″). The directions of dendritic planar projection thus correlated with the type-specific axonal locations. A pairwise comparison of dendritic traces of the same and different neuronal types revealed that determining the direction of planar projection of dendrites was sufficient to differentiate Tm2 and Tm9 from Tm20 (Figure S5B). Third, the dendritic terminals of all three Tm types were confined in or close to their cognate columns in essentially all layers (Figures 3E–3E″). This one-to-one correspondence between Tm neuron dendrites and medulla columns is consistent with these neurons' functions in receiving and processing retinotopic information.

Canonical Activin Signaling Regulates Dendritic Termination in Tm20 Neurons

To identify genes required for the proper dendritic patterning of Tm neurons, we screened a collection of known mutations for Tm20 dendritic morphological phenotypes and identified a *babo* null mutation (*babo*^{9}) (Zheng et al., 2003). The type I Activin/transforming growth factor β (TGF-β) receptor Baboon mediates Activin signaling in R7 photoreceptor axons and cultured S2 cells (Ting et al., 2007; Zheng et al., 2003). By using the MARCM technique (mosaic analysis with a repressible cell marker; Lee and Luo, 1999), we generated wild-type and *babo* mutant Tm20 clones and examined their dendritic patterns in adult animals. Unlike the wild-type, whose dendrites clustered around the photoreceptor axons in their cognate column (0% defect [n = 78]; Figures 4A, 4A′, 5A, and 5A′), mutant Tm20 neurons extended their dendrites laterally in the M3a layer and invaded neighboring columns (Figures 4B, 4B′, 5B, and 5B′; 100% [n = 29] of *babo*^{52}; 95.4% [n = 109] of *babo*^{9}). Furthermore, the mutant dendritic branches in the internal medulla M8 layer exhibited a similar overextension phenotype (100% for both *babo*^{9} [n = 109] and *babo*^{52} [n = 29]; Figures 4B and 4B′), suggesting that the lack of Baboon and, hence, the inability to respond to Activin/TGF-β signaling caused a global dendrite overextension phenotype in Tm20 neurons. The morphological phenotype was limited to dendrites, since the mutant Tm20s' axons were correctly targeted to the fifth layer of the lobula (data not shown).

Because the hs-Flp/MARCM technique generated random mutant cells that included both Tm20 and non-Tm20 cells, it remained formally possible that Baboon acts through neighboring cells to affect Tm20 dendrite development indirectly. To test the cell-autonomous function of Baboon in Tm20, we carried out the reverse MARCM experiments (Lee et al., 2000) and found that the wild-type Tm20 neurons that were presumably neighboring the *babo* mutant cells exhibited no observable dendritic phenotypes (0% [n = 79] of *babo*^{9}; data not shown). Next, we carried out transgene-mediated rescue experiments. Because the Gal4 driver by itself is not active early enough for transgene rescue, we therefore developed a concatenated split-LexA/MARCM system in which the ubiquitous Actin-Gal4 driving the rescue transgene and a GFP reporter in the MARCM mutant clones is coupled with the split-LexA system to mark mutant Tm20 clones with red fluorescent protein (RFP) (see Experimental Procedures for details). Using this system, we found that the transgene-mediated expression of the Baboon-A isoform fully rescued the *babo*^{9} dendritic phenotype of Tm20 (Figures 4E and 4E′; 0% defect, n = 66). Together, these results indicated that the Activin/TGF-β receptor Baboon is cell autonomously required in Tm20 neurons for their proper dendritic patterning.

To further characterize the dendritic phenotypes of *babo* mutant Tm20, we carried out dual-view imaging and morphometric analyses. We found that the *babo*^{9} mutant Tm20 neurons had fewer segments, longer averaged segment lengths, and larger dendritic trees, as compared with those of wild-type

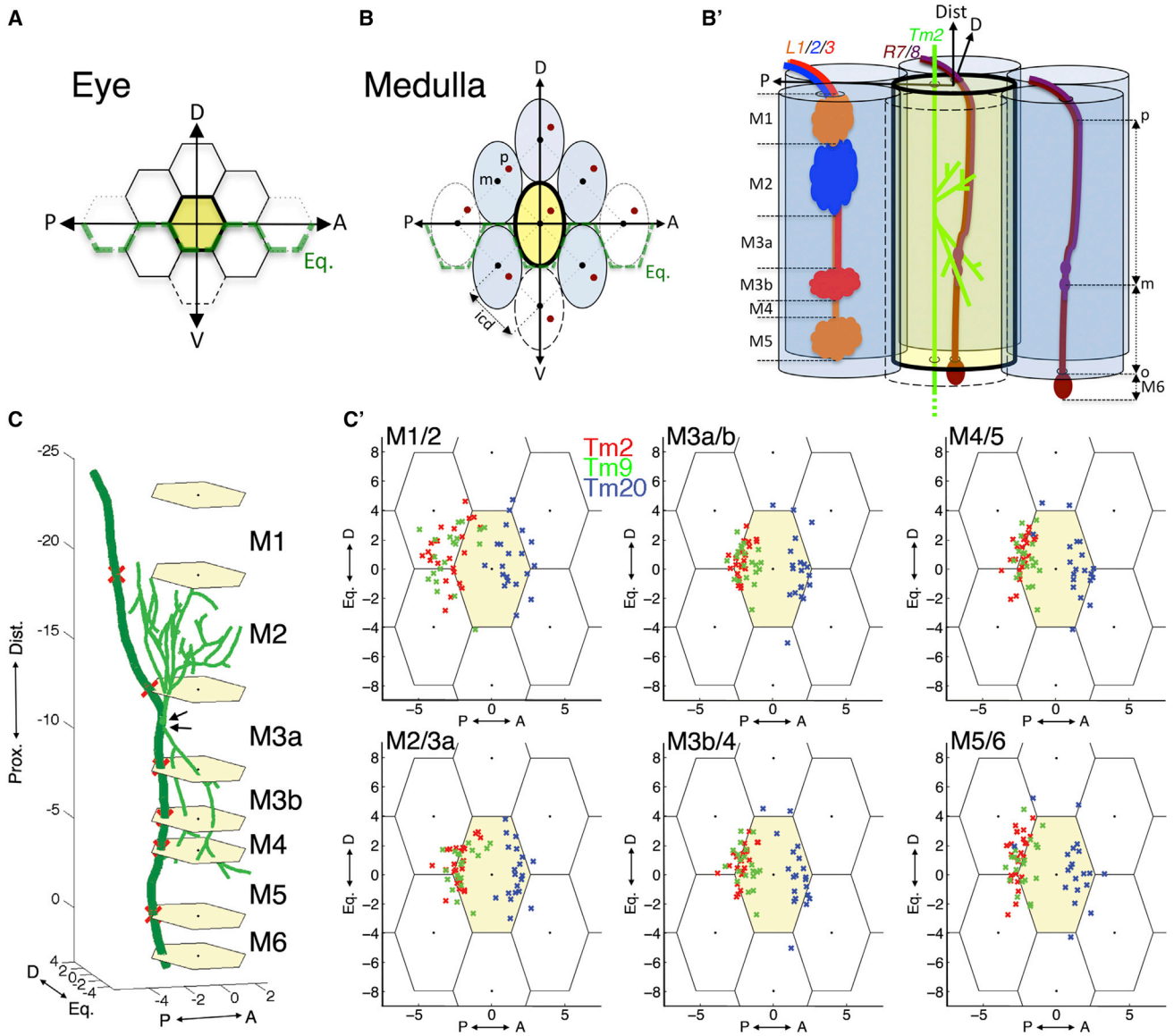

Figure 2. Registration and Standardization of Dendritic Trees

(A–B′) Schematic representations of the hexagonal ommatidial array in the eye (A) and the rhombic column array in the medulla (B) used for registration. In both the eye and medulla, an equator (green dotted lines) forms a mirror-symmetry plane that divides the dorsal (D) and ventral (V) portions. (B) shows a proximal-distal view of the medulla column array. (B′) shows the medulla columns in the dorsal-ventral view. The terminals of L1 (orange), L2 (blue), and L3 (red) lamina neurons and R7 photoreceptors were used to demarcate medulla layers M1/M5, M2, M3b, and M6, respectively. R7 (red) and R8 (purple) axons enter the medulla column at the anterior-dorsal or posterior-dorsal sides (red dots labeled "p") and curve to the middle of the columns in layers M3–M6 (labeled "m" and "o"). A Tm2 neuron is shown (green). icd, intercolumn distance. Distal (Dist), dorsal (D), and posterior (P) are as indicated.

(C and C′) The axonal positions of Tm2, Tm9, and Tm20 in the medulla columns are stereotypic. In (C), a registered Tm2 neuron and its cognate column (yellow hexagon) are shown in 3D. Arrows mark the parental nodes in the M3a layer, where dendrites branched from the axon. In (C′), the skeletonized neurites of Tm2 (red), Tm9 (green), and Tm20 (blue) were registered to the reference columns, and the axonal positions at layer boundaries (M1/2/3a/3b/4/5/6) were plotted with respect to the cognate columns (center yellow hexagons) in which their dendrites ramified. Tm2 and Tm9 axons were located at the posterior side of the column, while Tm20 axons were at the anterior.

See also Figure S4.

neurons (n = 20; Figures S3D–S3G). These results suggested that *babo* mutations might affect the branching/terminating properties of dendrites. The other metrics, including branching geometry, global contraction, and symmetry, were comparable between the wild-type and *babo* mutants (Figures S3H–S3O). Kaplan-Meier estimates further revealed that the dendritic terminating frequency of *babo* mutant Tm20 was significantly reduced (0.431 events per micrometer), although the dendritic branching

frequency was only mildly affected (0.322 events per micrometer), as compared with wild-type (Figures 4F and 4G). Examining the registered dendritic trees revealed that the axonal locations (data not shown) and the dendrite planar projection patterns of *babo* mutant Tm20 are comparable to those of wild-type (Figures 3D″ and 4J), while the percentage of dendritic branches terminating in the M3a layers increased by approximately 12% (Figures 3B″ and 4H). Together, these results indicated that the *babo* mutations reduced the dendrite termination frequency and mildly affected their distribution within medulla layers.

The lateral extension of dendrites in multiple medulla layers and the reduced dendrite termination frequency observed in *babo* mutant Tm20 suggested the Activin/TGF-β signaling pathway might have a global effect on these neurons' dendritic patterning. We therefore examined the involvement of dSmad2, a transcription factor that is the substrate of Baboon and that, in response to Activin, regulates transcription (Zheng et al., 2003; Ng, 2008). We found that the *dSmad2* null (*dSmad2^{F4}*) mutant Tm20 clones displayed essentially all the dendritic patterning phenotypes seen in *babo* mutants, including the characteristic lateral extension of dendrites in the M3a and M8 layers (Figures 4C and 4C′), reduced total segment numbers, increased average segment lengths (Figures S3D and S3E), and reduced dendritic termination frequency (0.488 events per micrometer; Figure 4G), with respect to the wild-type.

To examine the possibility that the observed dendritic phenotypes reflected cell-fate transformation, we examined the expression of cell-type-specific transcription factors in wild-type and mutant Tm20 neurons. A recent study revealed that a temporally regulated transcription factor cascade drives the development of diverse medulla neuronal types and that late-stage neuroblasts expressing the transcription factor Sloppy Paired or Dichaete give rise to Tm20 neurons, which express the transcription factor Toy (Twin of eyeless) but not Dichaete (Li et al., 2013). We found that *babo* mutant Tm20s, as well as their wild-type controls, expressed Toy but not Dichaete (Figure S6), suggesting that they retained their normal cell fate. Furthermore, both *babo* and *dSmad2* mutant Tm20 neurons targeted their axons correctly to the Lo5 layer (data not shown). Together, these results indicate that the canonical Activin/TGF-β signaling pathway regulates dendritic patterning but not cell fate or axonal targeting in Tm20 neurons.

Mutant Tm20 Neurons Devoid of Activin/TGF-β Signaling Form Aberrant Synaptic Contacts with Multiple Photoreceptors in the Neighboring Columns

Because mutant Tm20 neurons devoid of Activin/TGF-β signaling exhibited expanded dendritic trees, we registered dendritic trees to the reference columns and examined their dendritic receptive field. As compared with wild-type whose dendritic terminals clustered with their cognate columns (Figures 5A, 5A′, and 5C), *babo* mutant Tm20 neurons extended their dendrites into neighboring columns (Figures 5B and 5B′), especially in the M2 and M3a layers (Figure 5D). To determine whether the mutant dendrites could potentially form aberrant synapses with neighboring photoreceptors, we examined membrane contacts between Tm20 dendrites and photoreceptor axons using the GRASP (GFP reconstitution across synaptic partners) method (Feinberg et al., 2008; Gordon and Scott, 2009). We expressed one membrane-tethered split-GFP component (CD4::spGFP1-10) in single-cell Tm20 MARCM clones and the other component (CD4::spGFP11) in all photoreceptors and examined the native fluorescence signals of the reconstituted GFP molecules at the contact points. In wild-type, multiple strong GRASP signals were detected at the apparent contacts between dendrites and photoreceptor axons within their cognate columns in the M1–M3 layers (100%, n = 29; Figures 5E, 5E′, and 5I), but no fluorescence was seen with the expression of either split-GFP component alone (data not shown). These findings are consistent with serial electron microscopic reconstruction studies showing that R8 presynaptic sites are distributed in layers M1–M3 (Takemura et al., 2008) and that each Tm20 receives direct synaptic inputs from a single R8 photoreceptor within its cognate column (Takemura et al., 2013). In about 31% of the wild-type cases, weak GRASP signals were also detected with neighboring photoreceptor axons in the posterior-equatorial columns, which are likely GRASP artifacts. In sharp contrast, for all the *babo* mutant Tm20 neurons, strong GRASP signals were detected in the axons of neighboring photoreceptors (100%, n = 21), in addition to those in their cognate columns, suggesting that the mutant Tm20s formed aberrant synapses with neighboring photoreceptors (Figures 5F and 5F′). Consistent with the analyses on the registered dendritic trees (Figures 5B′ and 5D), the aberrant contacts were present most frequently in the two posterior (posterior-dorsal and posterior-equatorial) columns (71.4% and 47.6%, respectively; Figure 5J).

To determine whether these membrane contacts constituted genuine synapses, we labeled R8 presynaptic sites with the active zone marker Brp::mCherry and examined apparent contacts between R8 axons and Tm20 dendrites by colocalization (Figures 5G–5H″). We found that about 55% of the membrane contacts (n = 135) between *babo* mutant Tm20 dendrites and neighboring R8 axons colocalized with Brp::mCherry signals (Figure 5J), suggesting that these contacts were on, or juxtaposed to, R8's presynaptic sites. In contrast, wild-type Tm20 dendrites made apparent contacts only with cognate R8 axons, and about 69% of these contacts (n = 123) are juxtaposed to Brp::mCherry punta (Figure 5I). Thus, the aberrant dendrites of *babo* mutant Tm20 neurons appeared to receive synaptic inputs from multiple neighboring R8 photoreceptors, which resulted in expanded receptive fields and distorted retinotopic maps.

Activin/TGF-β Signaling Restricts the Dendritic Field of Wide-Field Dm8 Amacrine Neurons

We next examined the effect of Activin signaling on the dendritic field of wide-field amacrine neurons, which extend dendrites in two dimensions. We previously demonstrated that the wide-field amacrine neuron Dm8 extends dendrites in the M6 layers, where they receive direct synaptic inputs from approximately 16 R7 photoreceptors (Gao et al., 2008). Using the double-stochastic GFP/RFP labeling method, we found that the dendrites of Dm8 neurons overlapped significantly with their neighbors (Figures 6A and 6B), consistent with our previous finding that a single R7 photoreceptor provides synaptic inputs to multiple Dm8 neurons (Gao et al., 2008). We next examined Dm8 dendritic

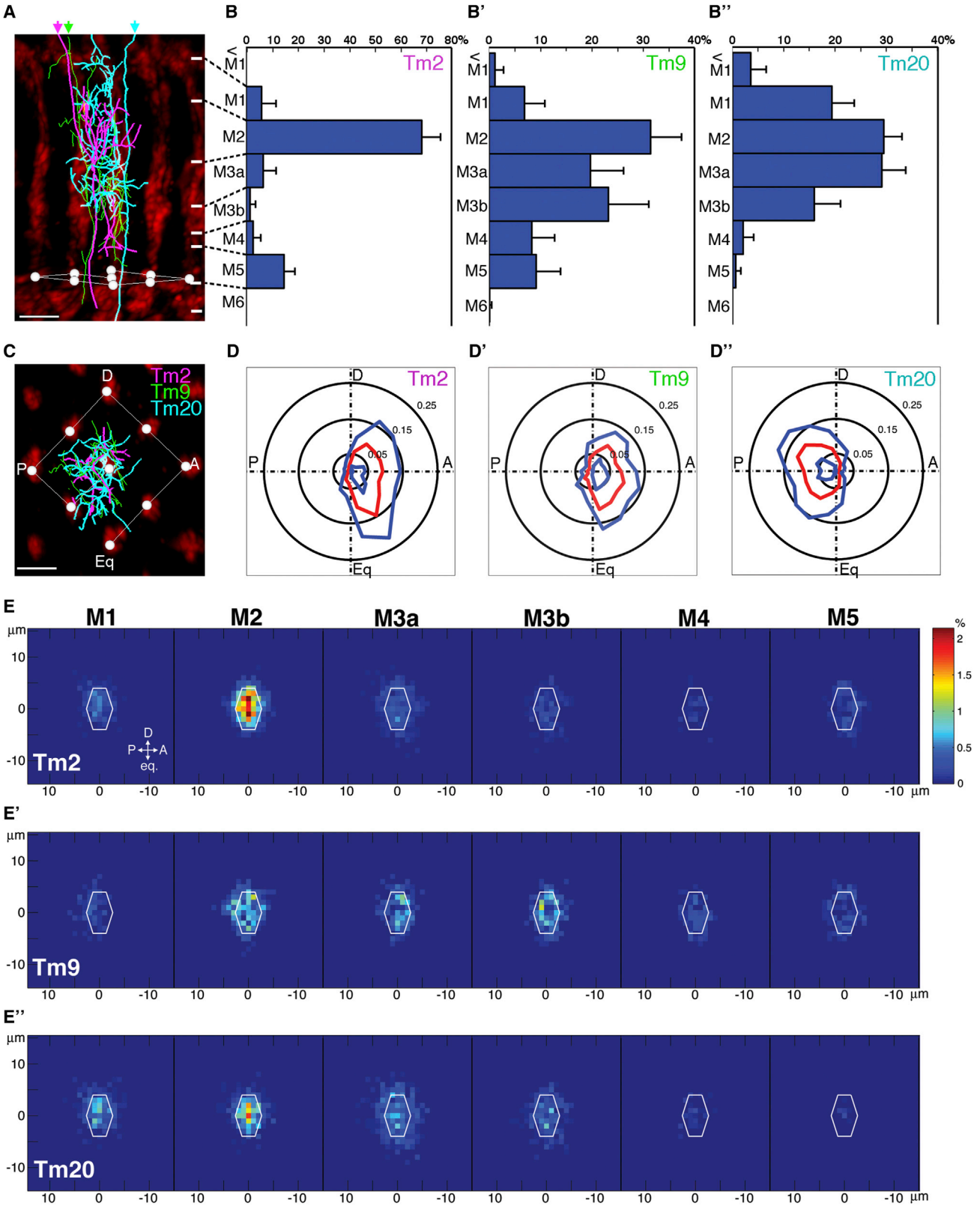

(legend on next page)

development using the flip-out mosaic technique. We found that, throughout development, the Dm8 dendrites remained in close proximity to R7 axons as soon as the axons arrived at the medulla neuropil in the early pupal stage (Figure S7). However, only at the second stage of medulla development (50%–70% after puparium formation) did Dm8 dendrites gradually spread within the M6 layer until they reached their adult size (Figure S7).

Because R7s express Activin (Figure 7A; Ting et al., 2007) and the R7 growth cones contact Dm8 dendrites throughout development, we set out to examine whether Activin signaling regulates Dm8 dendritic patterning. We found that *babo* mutant Dm8 dendrites seemed to encompass a larger space than the wild-type ones (Figures 6D and 6D′). To quantify the dendritic field, we counted the number of dendritic field units ([dfu] defined as a rhombus area with four neighboring photoreceptor terminals as vertexes; Figure 6C) occupied by the dendrites of single Dm8 neurons. We found that *babo* mutant Dm8 dendrites occupied significantly more dfu (20.1 ± 2.0; n = 28) than the wild-type ones (16.8 ± 1.2; n = 37; Figure 6G). Similarly, *dSmad2* mutant Dm8 had an expanded dendritic field (20 ± 1.6; n = 24; Figures 6E, 6E′, and 6G). Conversely, the ectopic expression of a dominant active form of Baboon ($Babo^{DA}$) in Dm8 significantly reduced the dendritic field sizes (13.8 ± 1.2; n = 17; Figures 6F, 6F′, and 6G) as compared to wild-type (Figures 6C, 6C′, and 6G). However, Dm8 neurons with either gain-of-function or loss-of-function *babo* mutations routes dendrites to the M6 layer, as in wild-types. These results indicate that the canonical Activin/TGF-β signaling pathway negatively regulates dendritic field size but not layer-specific ramification in Dm8.

Photoreceptor-Derived Activin Restricted the Dendritic Fields of Tm20 and Dm8 Neurons

The Activin receptor Baboon in *Drosophila* has four potential ligands: Activin, Dawdle, Myoglianin, and Maverick (Zheng et al., 2003; Parker et al., 2006; Awasaki et al., 2011; Gesualdi and Haerry, 2007). To identify the ligand for Tm20 and Dm8 and determine its source, we examined the mRNA expression patterns of these four ligands by RT-PCR and in situ hybridization. RT-PCR readily detected the expression of *Activin* and *Maverick* mRNA in pupal eye discs and *Maverick* mRNA in pupal brains (Figures S8A and S8A′). The *Activin in situ* signal was found abundant in R7 and R8 photoreceptors (Figure 7A), but the signal was much weaker in the developing medulla and lobula cortex (Figures S8C and S8C′). In contrast, the *Maverick in situ* signal was stronger in the developing lobula cortex than in the medulla cortex (Figures S8E and S8E′).

Insofar as the expression patterns pointed to photoreceptor-derived Activin as the most likely source of the Baboon ligand for Dm8 and Tm20 neurons, we first examined whether Activin was required for the Dm8 dendritic patterning. We used eye-specific GMR-Gal4 to drive the expression of Activin RNAi and examined the dendritic morphologies of otherwise wild-type Dm8 neurons using a LexA-based flip-out system (see Experimental Procedures). Knocking down Activin in the developing photoreceptors caused the Dm8 dendritic field to expand (18.8 ± 1.2 dfu; n = 26; Figures 7B and 7F), as with *babo* mutant Dm8 neurons. To differentiate between R7 and R8 as the source of Activin for Dm8, we genetically ablated R7 photoreceptors using the *sevenless* mutation. In the absence of R7s, Dm8 neurons showed expanded dendritic fields (20 ± 1.8 dfu; n = 18; Figures 7D and 7F), suggesting that R7 is required for their restriction. Furthermore, the ectopic expression of a dominant active form of Baboon ($Babo^{DA}$) in Dm8 in the *sevenless* background reduced the size of their dendritic fields (14 ± 1.9 dfu; n = 13; Figures 7E and 7F), suggesting that Baboon is downstream of R7-derived Activin. As in the *babo* mutants, in the absence of Activin or R7s, Dm8 dendrites still ramified in the M6 layer, indicating that neither is required for the layer-specific routing of Dm8 dendrites (data not shown). Conversely, overexpressing Activin in the developing photoreceptors with glass multiple reporter (GMR)-Gal4 further reduced the size of the Dm8 dendritic fields, compared with wild-type (14.3 ± 1.3 dfu; n = 17; Figures 7C and 7F). Together, these results indicated that R7-derived Activin plays an instructive role in restricting the Dm8 dendritic field.

We next examined whether photoreceptor-derived Activin regulates Tm20 dendritic patterning. RNAi-mediated knockdown of Activin in photoreceptors caused abnormal dendritic patterning in about 20% of the Tm20 neurons: that is, Tm20 dendrites failed to remain in their cognate column and, instead, extended into neighboring columns (19.8%, n = 81; Figures 7G–7G″). The incomplete penetrance of phenotypes suggests that photoreceptor-derived Activin is partially required for proper dendrite patterning of Tm20. In contrast to the requirement for R7s to correctly pattern the Dm8 dendrites, ablating R7s had no effect on the Tm20 neurons' dendrite patterning (data not shown), suggesting that R8s might be the source of the requisite

Figure 3. Dendritic Attributes Revealed by Registration to the Reference Columns

(A–D″) Tm dendrites project to specific medulla layers shown in (A)–(B″) in stereotyped planar orientations shown in (C)–(D″). Tm2 (magenta), Tm9 (green), and Tm20 (blue) dendrites were registered to the reference columns and are shown in dorsal-ventral (A) and proximal-distal views (C). Arrows marks the axons of Tm neurons. Photoreceptor axons (red), labeled with the 24B10 antibody, were used for landmarks, and the R7 axons at the M5/M6 boundary are labeled with white dots. Scale bars, 4 μm.

(B–B″) The dendrites of Tm neurons show stereotyped layer distributions. The averaged fractions of dendritic terminals in different medulla layers are plotted as bar charts. Error bars represent SDs.

(D–D″) The planar projection directions of Tm dendrites (calculated as vectors from parental nodes to terminal nodes) are shown as polar plots. Red and blue lines represent means and SDs, respectively. Tm2 (D) and Tm9 (D′) dendrites projected anteriorly to innervate their cognate columns, and Tm20 (D″) dendrites projected posteriorly.

(E–E″) The dendritic arbors of Tm neurons were largely confined to single medulla columns. The distributions of the dendritic terminals of Tm2 (E), Tm9 (E′), and Tm20 (E″) through layers M1–M5 are shown as heat maps. The central white hexagons mark the cognate columns, i.e., the primary columns innervated by Tm dendrites. The density of the dendritic terminals of each neuron was calculated at the resolution of 1 μm × 1 μm for each layer and is displayed as the averaged fraction of the total terminal number. The color bar displays the color range of the averaged fractions. Orientations are as indicated: D, dorsal; Eq, equatorial; P, posterior; A, anterior.

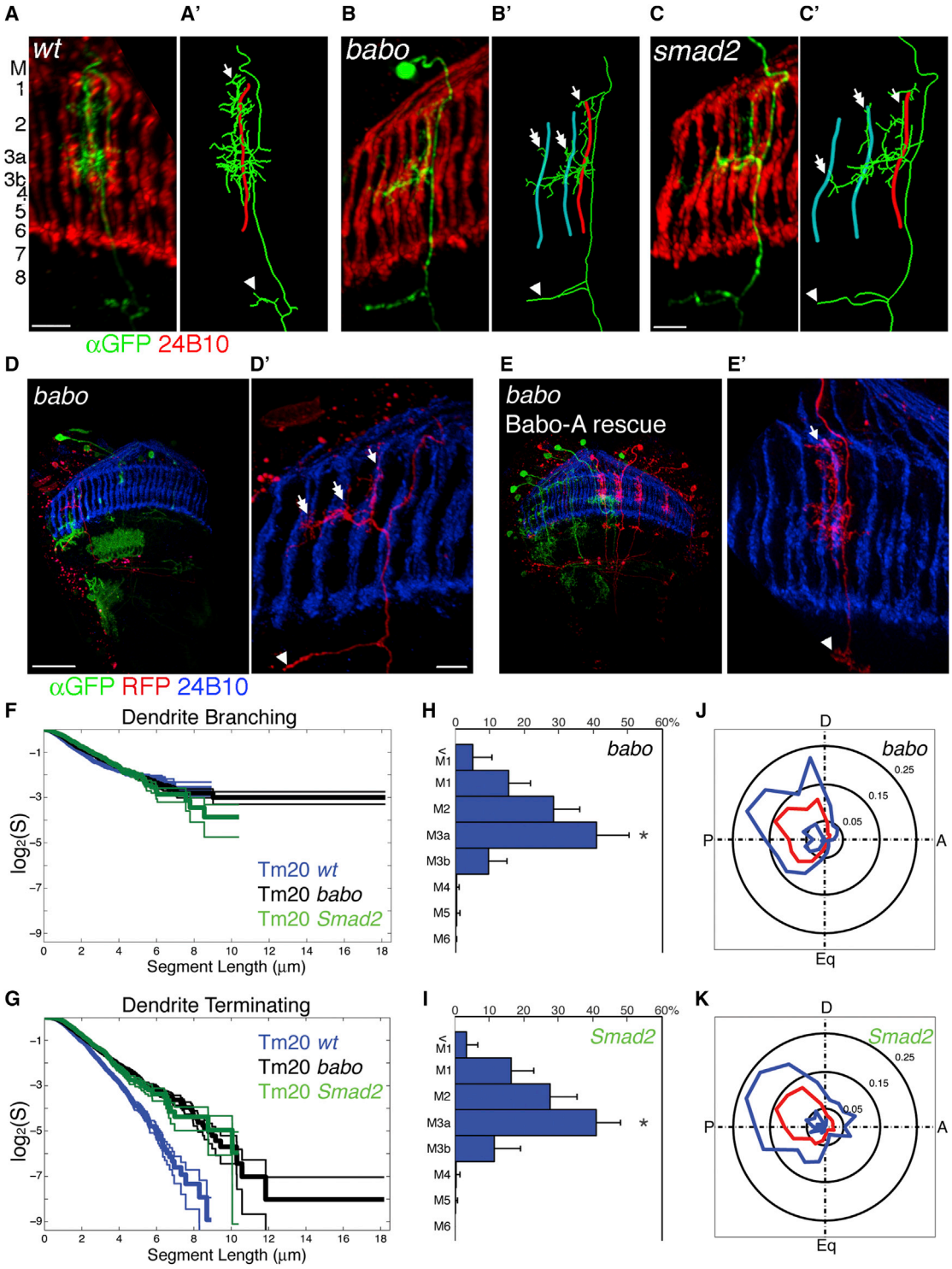

Figure 4. The Canonical Activin/TGF-β Signaling Pathway Regulates Tm20 Dendritic Patterning

(A–E′) The type I Activin/TGF-β receptor Baboon and its downstream transcription factor dSmad2 are cell-autonomously required in Tm20 for normal dendritic patterning. mutant Tm20 neurons—single wild-type (WT) in (A) and (A′), *babo* in (B) and (B′), and *dsmad2* in (C) and (C′)—were generated by the MARCM method. Their dendrites, labeled with the mCD8GFP marker (green), were examined for morphological defects. Photoreceptors axons, visualized by the 24B10 antibody (red), were used as landmarks. In (A′), (B′), and (C′), traced dendrites (green) and the photoreceptor axons in the cognate column (red) and neighboring columns (cyan) are shown. (A) and (A′) show wild-type Tm20 dendrites (arrow) clustered around a single R8 photoreceptor axon (red).

(legend continued on next page)

Activin for Tm20. Because ablating R8 would severely disrupt the development of eye discs and optic lobes (Jarman et al., 1994; Kunes and Steller, 1991), we tested the involvement of R8s by overexpressing the transmembrane receptor Golden Goal in developing photoreceptors. The overexpression of Golden Goal stalled the extension of the R8 axons in the M1 layer, thus preventing them from reaching the M3 layer (Tomasi et al., 2008). In the absence of R8 terminals in the M3 layer, the Tm20 dendrites exhibited dendritic patterning defects (36%, n = 50) similar to those caused by Activin RNAi (Figures 7H–7H″). Kaplan-Meier estimates further revealed that their dendrite terminating frequency is reduced (0.539 ± 0.011 events per micrometer) as compared with wild-type (0.594 events per micrometer) but more modestly than the *babo* mutants (0.430 events per micrometer). Ablating the R7s did not modify this dendritic phenotype (data not shown), suggesting that R7 is not redundant with R8 for proper Tm20 dendrite patterning. The combination of stalling R8 axons and expressing Activin RNAi in photoreceptors also did not significantly enhance this dendritic phenotype (32.6%, n = 49; data not shown). Finally, R8-specific Acitivn knockdown caused similar but somewhat weaker dendritic patterning defects in Tm20 (20.8%, n = 53; Figures 7I–7I″). Taken together, these results suggest that R8-derived Activin is partially required for proper Tm20 dendrite patterning.

DISCUSSION

Drosophila Medulla Neurons Serve as a Model for Studying Dendrite Development and Synaptic Specificity in the CNS

Studies of the past decade have revealed the molecular mechanisms by which photoreceptor and lamina axons target to specific medulla layers, as well as those mechanisms restricting their axonal terminals to their retinotopic columns (reviewed in Melnattur and Lee, 2011). However, obtaining comparable information on their synaptic partners, the dendrites of the medulla neurons, has been stymied by the morphological complexity of the dendrites and the lack of genetic and analytical tools. Here, we reported techniques for visualizing and analyzing the dendritic structures of the medulla neurons. The dual-imaging technique reported here requires only regular confocal microscopes to generate 3D images of dendrites, and the registration method exploits the regular array structure of the medulla to permit the standardization of dendritic patterns for analyses. In addition, recent studies have begun to unravel the transcription programs that govern the development of diverse medulla cell types (Li et al., 2013), and serial electron microscopy reconstruction studies have illustrated their complex synaptic circuits (Takemura et al., 2013; Gao et al., 2008). These advances are paving the way to studies on dendrite patterning in 3D space and the establishment of synaptic partnerships between axons and dendrites in the *Drosophila* medulla.

Type-Specific Dendritic Attributes of Tm Neurons Are Directly Related to the Medulla Layer and Column Structure

Our morphometric analyses of Tm neurons revealed dendritic properties distinct from those of the da sensory neurons in the peripheral nervous system. Different classes of da neurons have distinguishable morphometric parameters, such as branching geometry, and their distinguishing dendritic morphological features are correlated with specific branching orders (Jan and Jan, 2010). In contrast, the three Tm neuron types have similar dendritic branching and terminating frequencies and share similar dendritic geometrical properties. As such, the standard morphometrics are ineffective in differentiating Tm types. Instead, the type-specific dendritic attributes of Tm neurons, revealed by registration, are directly related to the layer and column structure of the medulla. These distinctions likely reflect the different functions that the dendrites of da and Tm neurons serve: da dendrites are free-ending sensory branches that tile the two-dimensional body wall, whereas Tm dendrites receive synaptic inputs from retinotopically directed afferents organized in layers and columns.

Our examination of the dendritic attributes of Tm neurons provides insights into how dendritic morphology is achieved in these neurons. The axons of Tm9 and Tm2 were localized to the posterior side of their cognate columns, and their dendrites extended anteriorly to innervate their cognate columns, while Tm20 axons were at the anterior side of the column and their dendrites projected posteriorly. These type-specific axonal localizations are probably a consequence of their ontogeny: Tm9 and Tm2 axons are fasciculated (Ting and C.-H.L., unpublished data), and these neurons are presumably derived from one cell lineage (or closely related ones) (Li et al., 2013). Layer-specific termination of dendrites, the most prominent type-specific attribute of medulla neurons, matches the layer-specific termination

(B–C′) Tm20 neurons lacking Baboon in (B) and (B′) or dSmad2 in (C) and (C′) arborized dendrites in their cognate columns (arrow) and neighboring columns (double arrows). In addition, their dendritic branches in the M8 layer (arrowhead) were longer, compared to those of the wild-type shown in (A) and (A′).
(D–E′) The dendritic phenotypes of *babo* mutant Tm20 neurons were fully rescued by expressing the Baboon-A isoform. *Babo* mutant Tm20 and other medulla neurons, generated by the hs-flp/MARCM system, were labeled by rCD2RFP (red) and mCD8GFP (green), respectively, using a concatenated Gal4/LexA dual expression system (see Experimental Procedures for details). Expressing the Baboon-A isoform in the *babo* mutant Tm20, as shown in (E) and (E′), rescued the *babo* mutant dendritic phenotypes, as shown in (D) and (D′), indicated by double arrows. (D′) and (E′) show high-magnification views of (D) and (E), respectively.
(F and G) The semi-log plots show the Kaplan-Meier estimates (S) of dendrite branching (F) and dendrite termination (G) in wild-type (blue), *babo* (black), and *dSmad2* (green) mutant Tm20 neurons. As compared with the wild-type, the dendritic termination KME curves of *babo* and *dSmad2* mutant Tm20s had shallower slopes, indicating a lower dendritic terminating frequency.
(H and I) Bar charts show layer distributions of the dendritic terminals of *babo* (H) and *dSmad2* (I) mutant Tm20s, which were similar to the wild-type arborizations (Figure 3B″), except in the M3a layer (asterisk). Error bars represent SDs.
(J and K) Polar plots show the planar orientations of dendritic projections from *babo* (J) and *dSmad2* (K) mutant Tm20 neurons, which were similar to that of the wild-type (Figure 3D″). Red and blue lines represent means and SDs, respectively.
Scale bars, 7 μm (A–B′), 5 μm (C, C′, D′, and E′), and 30 μm (D and E).

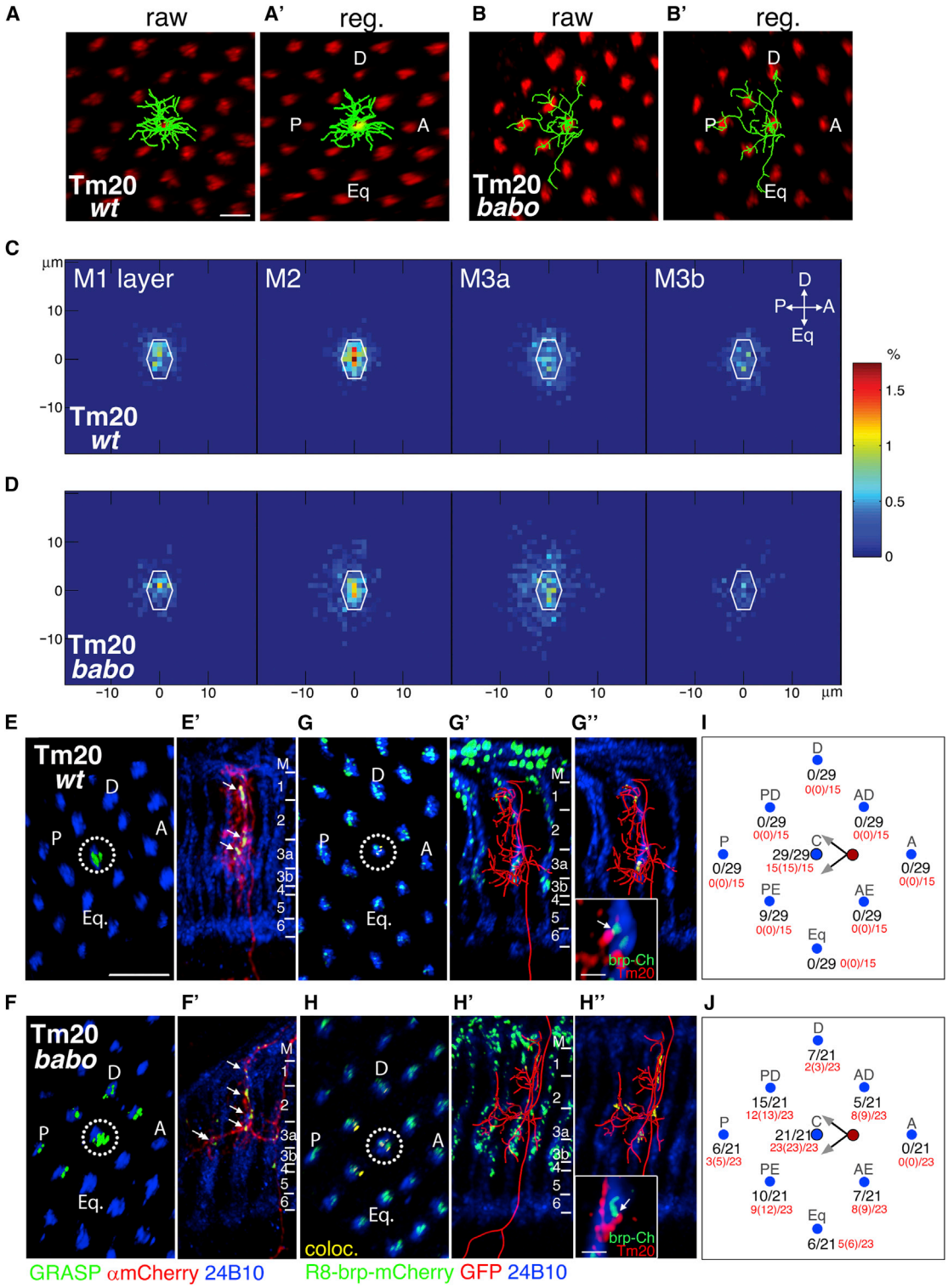

Figure 5. Tm20 Neurons Devoid of Activin Signaling Exhibit Expanded Dendritic Fields and Form Aberrant Synapses with Multiple Photoreceptors in the Neighboring Columns

(A–B′) Proximal-distal views of the dendrites of wild-type (WT) and *babo* mutant Tm20 neurons. Single wild-type (A and A′) and *babo* mutant (B and B′) Tm20 neurons were generated and labeled with the mCD8GFP marker (green) using the MARCM technique. The dendrites were traced in (A) and (B) and registered to the reference columns in (A′) and (B′). Photoreceptor axons, labeled with the 24B10 antibody, were used as landmarks. *Babo* mutant Tm20 neurons extended dendrites to innervate multiple neighboring columns. Scale bars, 5 µm. D, dorsal; P, posterior; raw, unregistered dendritic tree; reg., registered dendritic tree.

(legend continued on next page)

of their presynaptic partners (Fischbach and Dittrich, 1989). Previous developmental studies have shown that columns and layers form as the different types of afferents sequentially innervate the medulla during development (Ting et al., 2005; Timofeev et al., 2012; Pecot et al., 2013). The observation that type-specific dendritic attributes are directly related to medulla layers and columns thus led to the hypothesis that different types of medulla neurons respond differentially to various afferent-derived cues to pattern dendrites.

Activin Signaling Restricts the Dendritic Fields of Columnar and Amacrine Neurons

In this study, we uncovered that Activin signaling regulates the dendritic field size of the columnar neuron Tm20 and the wide-field amacrine neuron Dm8. TGF-β family morphogens have been shown to regulate a broad range of neurodevelopmental processes, including proliferation and cell-fate determination during early stage of development (O'Connor et al., 2006), as well as the promotion of axonal development through a noncanonical pathway involving Lim kinase (Ng, 2008). In this study, we found that Activin signals through the canonical pathway to regulate dendritic patterning in Tm20 and Dm8 neurons: the transcription factor dSmad2 was functionally required for Activin-dependent dendritic patterning, and the lack of Activin signaling caused a global dendritic phenotype.

The specificity of Activin signaling in regulating dendritic patterning is underscored by the distinct dendritic patterning defects, as well as the absence of cell-fate transformation and axonal targeting defects, observed in mutant neurons. Activin-signaling-deficient Tm20 neurons still expressed the appropriate transcription factors and markers and projected their axons to the correct target layer in the lobula; mutant Dm8 elaborated their dendrites in the appropriate medulla layer M6. Instead, lack of Activin signaling reduced dendritic terminating frequency and expanded dendritic fields, while the planar projection orientations and layer-specific terminations were largely unaffected. We speculate that Activin signaling leads to the transcription regulation of an as-yet-unidentified factor (or factors) that facilitate the termination of dendritic arbors.

Several lines of evidence suggest that Activin for Tm20 and Dm8 is, at least in part, provided by their respective presynaptic partners, R8 and R7. R7 and R8, but not R1-R6, expressed Activin during pupal stages, and RNAi-mediated knockdown of Activin in photoreceptors resulted in expanded dendritic fields in the Dm8 and Tm20 neurons. The cell-specific requirement for Activin is underscored by the observations that the genetic ablation of R7s phenocopied *babo* in Dm8 but not in Tm20 neurons and that stalling R8 axons in the superficial M1 layer (thereby preventing the delivery of R8-derived Activin to the M3 layer) and Activin knockdown in R8s disrupt the normal dendritic patterning of Tm20. We note that either Activin-RNAi or R8 stalling caused milder Tm20 dendritic phenotypes than did removing Baboon but that their combination did not significantly enhance Tm20 dendritic phenotypes. Thus, there is likely a secondary and partially redundant Activin source—for example, other medulla neurons—for Tm20. Nonetheless, the specific requirement of afferents indicates that R8-derived Activin cannot substitute for that from R7s, and vice versa, even though these terminals reside only a few micrometers apart. We therefore suggest that R7- and R8-derived Activin functions, in a short-range or layer-restricted fashion, to regulate the dendritic patterning of Dm8 and Tm20, respectively (Figure 8).

Photoreceptor-derived morphogens, such as hedgehog, EGF, and Jelly Belly, have been shown to act, in an anterograde fashion early in development, to regulate the proliferation and differentiation of their target area (Huang et al., 1998; Huang and Kunes, 1996; Bazigou et al., 2007). Our current finding, that photoreceptor-derived Activin regulates the dendrite development of their synaptic targets, further suggests anterograde signaling as an effective mechanism for coordinating afferent-target development, even late in development. The wide-field neuron Dm8, which mediates innate UV preference, pools approximately 16 R7 inputs and relays the information to a few Tm5c neurons in the center of their dendritic field (Gao et al., 2008; T.Y.L. and C.-H.L., unpublished data), while the Tm20 neurons form synapses in one-to-one correspondence with R8s and process retinotopic information. Conceivably, the

(C and D) Heat maps show the distributions of the dendritic terminals of wild-type (C) and *babo* mutant (D) Tm20 neurons in layers M1–M3b (as shown). The color bar displays the color range of the averaged fractions. As compared to wild-type (C), the dendritic terminals of *babo* mutant Tm20 neurons (D) extended into the neighboring columns in the M2 and M3a layers.
(E–F′) Membrane contacts between Tm20 dendrites and photoreceptor axons were assessed using the GRASP method. Tm20 neurons—single wild-type in (E) and (E′) or *babo* mutant in (F) and (F′)—were generated by the MARCM method and marked with one split-GFP component (CD4::spGFP1-10) and the mCD8-mCherry marker (red). Photoreceptor terminals were labeled with the other split-GFP component (CD4::spGFP11) and counterstained by the 24B10 antibody (blue). The reconstituted GFP was detected by its native fluorescence (green) at the apparent contacts between Tm20 dendrites and photoreceptor axons. While multiple strong GFP signals (arrows) were detected in the cognate photoreceptor axons (dotted circles) for Tm20 neurons, both wild-type in (E) and (E′) and *babo* mutant in (F) and (F′), additional strong GFP signals were found in the neighboring photoreceptor axons for the mutant Tm20 (double arrow), shown in (F) and (F′).
(G–H″) Contacts between R8 presynaptic sites and Tm20 dendrites were assessed by confocal microscopy and colocalization. R8 presynaptic sites were labeled by the active zone marker Brp::mCherry (pseudocolored in green), and photoreceptor axons were counterstained by the 24B10 antibody (blue). Tm20 neurons—single wild-type in (G)–(G″) and *babo* mutant in (H)–(H″)—generated by MARCM were labeled with the mCD8::GFP membrane marker, and their dendrites were traced (red). In (G″) and (H″), presumptive synaptic contacts (yellow) between R8 presynaptic sites and Tm20 dendrites were identified by colocalization. While wild-type Tm20 dendrites form contacts exclusively with the presynaptic sites of the cognate R8s, *babo* mutant Tm20 dendrites contacted the presynaptic sites of both cognate and neighboring R8s. Insets show high-resolution views of the presumptive synaptic contacts (arrows). (E), (F), (G), and (H) show proximal-distal views; (E′), (F′), (G′), and (H″) show dorsal-ventral views. Scale bars, 10 μm for (E–H″) and 2 μm (G″ and H″, insets).
(I and J) Summary of the dendritic contacts with axons from the cognate (labeled as C) and eight neighboring photoreceptors shown in the proximal-distal view. The GRASP results in (E) through (F′) are displayed in black numbers (number of Tm20-contacted photoreceptors/number of Tm20s examined), and the presumptive synaptic contacts in (G)–(H″) are displayed in red (number of Tm20-contacted R8 presynaptic sites [number of Tm20-contacted R8 axons]/number of Tm20s examined).

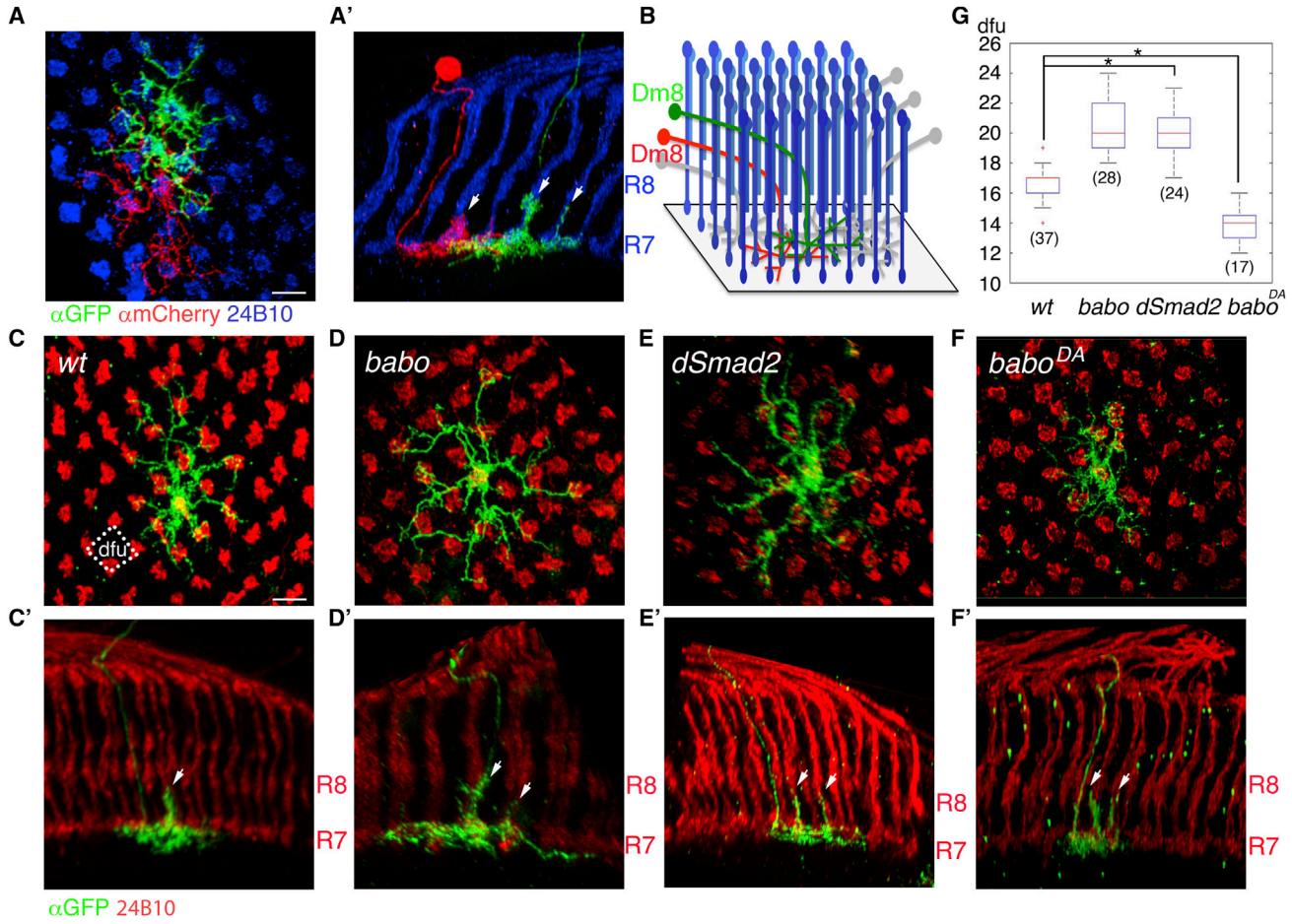

Figure 6. Baboon Activity Controls the Dendritic Field Sizes of Dm8 Amacrine Neurons

(A–B) Neighboring Dm8 neurons show extensive overlapping dendritic fields. Single Dm8 neurons were separately labeled by mCD8-GFP (green) or rCD2-mCherry (red), using the double stochastic labeling method. Dm8 neurons extended large dendritic processes in the M6 layer, which extensively overlapped with dendrites from neighboring Dm8 neurons. In addition, each Dm8 neurons extended small centrifugal processes to the M4 layer (arrows). Photoreceptor axons, labeled by the 24B10 antibody (blue), were used as landmarks. (A) Proximal-distal views. (A′) Dorsal-ventral views. (B) shows a schematic illustration of (A). Unlabeled Dm8 neurons are in gray. Scale bar, 5 μm (A and A′).

(C–E) Mutant Dm8 clones—single wild-type (WT) in (C) and (C′), *babo* in (D) and (D′), and *dSmad2* null in (E) and (E′)—were generated and labeled with the mCD8GFP marker (green) using the MARCM technique. Photoreceptor axons were visualized by the 24B10 antibody staining (red). In (D) and (E), as compared with wild-type, *babo* and *dSmad2* null mutant Dm8 neurons elaborated larger dendritic fields, covering more dendritic units. A dfu was defined as a rhombus area, indicated by dotted lines in (C), with four neighboring photoreceptor terminals as vertexes.

(F and F′) Dm8 neuron ectopically expressing a dominant-active form of Baboon had a smaller dendritic field as compared with wild-type ones.

(G) Box plot showing the dendritic field sizes of wild-type, *babo* null, *dSmad2* null, and *babo* gain-of-function mutant Dm8 neurons. The edges of the boxes are the first and third quartiles, and red lines marked the medians. Outliners are displayed as red crosses. *$p < 0.05$; Student's t test.

(C′), (D′), (E′), and (F′) show dorsal-ventral views of (C), (D), (E), and (F), respectively. Scale bar, 5 μm (C–F′).

formation of appropriate dendritic field sizes and the correct synaptic partnership is critical for the functions of Tm20 and Dm8 neurons. We reason that the dendritic tiling mediated by mutual repulsion, an important regulatory feature of the da neurons, alone is not suitable for restricting Tm20s' and Dm8s' dendritic fields because Tm20's dendrites arborized in 3D space and Dm8's dendrites overlap extensively with that of their neighbors. The use of afferent-derived Activin to regulate dendritic patterning provides an adaptable and self-compensating mechanism for afferents to control the dendritic field sizes of their synaptic targets.

EXPERIMENTAL PROCEDURES

Genetics

Fly stocks were maintained on standard fruit fly medium at 25°C. Transgenic flies were generated using a standard P-element or PhiC31-mediated transformation protocol by Rainbow Transgenic Flies, Inc. The fly stocks are listed in the Supplemental Experimental Procedures.

Molecular Biology

Transgenic constructs were generated by standard subcloning, PCR, and in-fusion cloning. For details, see the Supplemental Experimental Procedures.

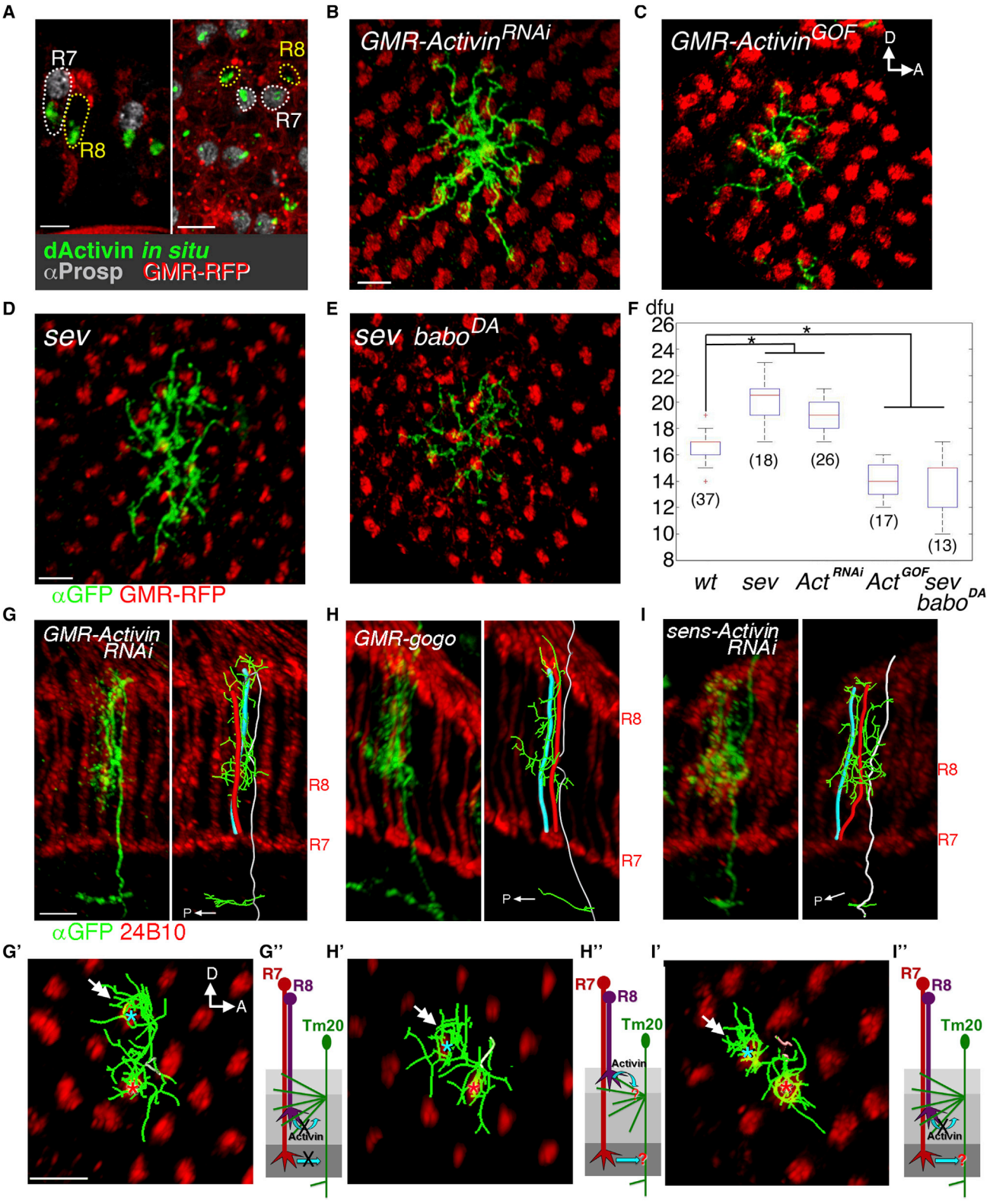

(legend on next page)

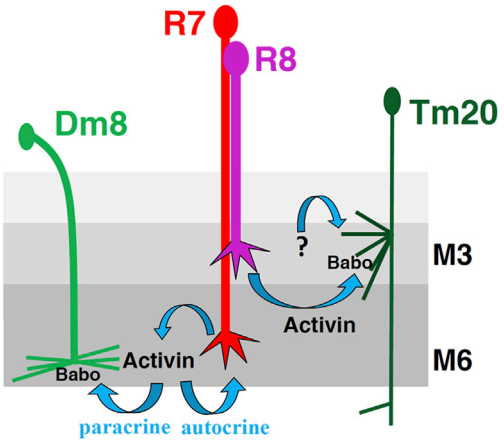

Figure 8. Schematic Model Illustrating the Restriction of Target Neurons' Dendritic Fields by Photoreceptor-Derived Activin

Activin derived from R8 photoreceptors promotes the dendritic termination of Tm20 neurons and restricts them to their cognate columns. There is likely a secondary and partially redundant Activin source for Tm20 (question mark). R7-derived Activin plays dual roles: anterograde signaling restricts the dendritic field of R7-target Dm8 neuron, and autocrine signaling restricts R7 growth cones to their retinotopically correct columns.

GRASP

GRASP for detecting membrane contacts between R8 and Tm20 was performed as described previously (Gordon and Scott, 2009). The native fluorescence signal of reconstituted GFP was used.

Immunohistochemistry

Immunohistochemistry was performed as described previously (Ting et al., 2007). Confocal images were acquired using an inverted Zeiss LSM510 Meta or an upright Zeiss LSM780 microscope. Detailed procedures are given in the Supplemental Experimental Procedures.

Dual-View Imaging

The dual-view imaging method combines two dual-channel 3D image stacks collected from two nearly orthogonal directions to reduce Z distortion in single 3D images. Both image stacks were deconvolved using the Huygens Professional package (Scientific Volume Imaging) running on a 64-core Fujitsu RX900 S1 with 1 TB memory. The two deconvolved image stacks were registered and then combined using a custom-made plug-in built into the open-source MIPAV programming environment (http://mipav.cit.nih.gov/). For details, see the Supplemental Experimental Procedures.

Tracing Dendrites

The recombined 3D images were rendered in 3D stereo using Imaris software (Bitplane) and a graph workstation equipped with a NVIDIA Quadro 3D vision system. Dendrites were traced using the semiautomatic method of the Imaris Filament Tracer module with manual track editing. The filament files were converted from the default inventor file format to the standard SWC file format by custom program coded in Java. Standard morphometric analyses were carried out using L-measure (Scorcioni et al., 2008). Segment analyses were carried out using custom programs coded in Matlab with the Trees toolbox (Cuntz et al., 2010). For details, see the Supplemental Experimental Procedures.

Registration of Dendritic Trees to the Reference Columns

Landmark-based registration methods, implemented in MIPAV (Medical Image Processing, Analysis, and Visualization), were used to register the combined 3D images and skeletonized dendritic trees to the reference columns. Using a set of 27 landmarks from the surrounding photoreceptor axons, we mapped the combined 3D images on to the reference column space. Custom Matlab scripts were used to analyze the registered dendritic trees for planar projection and layer-specific arborization. An appropriate mirror symmetry operation was applied to the registered dendritic trees for the data collected from the ventral half of the right optic lobe and the dorsal half of the left optic lobe. For details, see the Supplemental Experimental Procedures.

Statistical Analysis

We applied the KME for incomplete observations to estimate the probability (S, Figures 1G, 1H, 4F, and 4G) that a dendritic segment of a given length will either branch or terminate (Kaplan and Meier, 1958). The Poisson probabilities for branching or terminating were calculated from pooled data for each

Figure 7. R7- and R8-Derived Activin Instructively Patterns the Dendrites of Dm8 and Tm20, Respectively

(A) Expression pattern of Activin in the late pupal eye disc. Activin mRNA (green) was detected in R7 and R8 cell bodies by in situ hybridization. Left: side view. Right: frontal view. R7 photoreceptors were visualized by labeling with the anti-Prospero antibody (gray). Cell membrane, visualized by a GMR promoter driving a membrane-associated RFP (GMR-myrRFP, red), was used to identify R8. Scale bars, 7 μm in right panel, and 5 μm in left panel.

(B–E) Proximal-distal views.

(B) RNAi-mediated knockdown of Activin in photoreceptors caused an expansion of the Dm8 dendritic field. The Dm8 dendrites (green) were assessed in adult flies carrying a GMR-Gal4-driven Activin RNAi construct. Photoreceptor axons were visualized by the 24B10 antibody (red).

(C) Overexpressing Activin in photoreceptors reduced Dm8 dendritic field size. The dendritic processes of Dm8, labeled by the mCD8GFP marker (green), were assessed in adult flies carrying a GMR-Gal4-driven Activin construct. D, dorsal; A, anterior.

(D) Genetic ablation of R7s using the *sevenless* mutation (sev) increased the Dm8 dendritic field. The dendrites of single Dm8 neurons were labeled by mCD8-GFP (green).

(E) A Dm8 neuron expressing a dominant active form of Baboon ($babo^{DA}$) in the *sevenless* background had a reduced dendritic field despite the absence of R7s.

(F) Box plot showing the dendritic field sizes of Dm8 neurons in wild-type and various mutant backgrounds. The edges of the boxes are the first and third quartiles, and red lines marked the medians. Outliners are displayed as red crosses. *$p < 0.05$; Student's t test.

(G–I″) In (G)–(I), left panels show the original confocal image, and right panels show the traced dendritic tree of the Tm20 neuron (green) and the photoreceptor axons in the cognate column (red) and neighboring column (cyan). (G′), (H′), and (I′) show proximal-distal views of (G), (H), and (I), respectively. (G″), (H″), and (I″) show schematic illustrations of (G), (H), and (I), respectively. In (G)–(G″), RNAi-mediated knockdown of Activin in the photoreceptors caused dendritic patterning defects in the Tm20 neurons. The Tm20 dendrites, labeled with the mCD8GFP marker (green) were assessed in adult flies carrying a GMR-Gal4-driven Activin RNAi construct. Tm20 neuron extended dendrites into the dorsal column (double arrow, blue star) in addition to its cognate column (red star). In (H)–(H″), stalling R8 axons in the M1 layer caused dendritic patterning defects in the Tm20 neurons. The dendrites of single Tm20 neurons (green) were assessed in adult flies carrying the GMR-Gal4 transgene driving the expression of Golden Goal (gogo), which prevented R8 axons from entering the M3 layer. The Tm20 neuron extended dendrites to its cognate column (red star) and the dorsal-posterior column (double arrow, blue star). In (I)–(I″), RNAi-mediated knockdown of Activin in the R8 photoreceptors caused dendritic patterning defects in the Tm20 neurons. The Tm20 dendrites, labeled with the mCD8GFP marker (green), were assessed in adult flies carrying a senseless-Gal4-driven Activin RNAi construct. Tm20 neuron extended dendrites into the dorsal-posterior column (double arrow, blue star) in addition to its cognate column (red star).

Scale bars, 5 μm (B–E and G–I′).

neuron type by linear regression using segments of 0.5–4 μm in length (Figures 1G, 1H, 4F, and 4G). All statistical methods were implemented using Matlab script with the Trees toolbox (Cuntz et al., 2010). For details, see the Supplemental Experimental Procedures.

SUPPLEMENTAL INFORMATION

Supplemental Information includes Supplemental Experimental Procedures, eight figures, and one table and can be found with this article online at http://dx.doi.org/10.1016/j.neuron.2013.12.012.

ACKNOWLEDGMENTS

We thank Xin Li, Claude Desplan, Shinya Takemura, and Dimitri Chklovskii for communicating results prior to publication; Tzumin Lee, Takashi Suzuki, and Claude Desplan for providing critical reagents; and Edward Giniger, Hari Shroff, Alexander Borst, and Alan Hinnebusch for helpful discussion. This work was supported by the Intramural Research Program of the National Institutes of Health, the Eunice Kennedy Shriver National Institute of Child Health and Human Development (grant HD008913 to C.-H.L.), the Center for Information Technology (P.G.M., N.P., and M.M), and R01 GM095746 to M.B.O.

Accepted: December 2, 2013
Published: January 23, 2014

REFERENCES

Awasaki, T., Huang, Y., O'Connor, M.B., and Lee, T. (2011). Glia instruct developmental neuronal remodeling through TGF-β signaling. Nat. Neurosci. *14*, 821–823.

Bazigou, E., Apitz, H., Johansson, J., Lorén, C.E., Hirst, E.M., Chen, P.L., Palmer, R.H., and Salecker, I. (2007). Anterograde Jelly belly and Alk receptor tyrosine kinase signaling mediates retinal axon targeting in *Drosophila*. Cell *128*, 961–975.

Cuntz, H., Forstner, F., Borst, A., and Häusser, M. (2010). One rule to grow them all: a general theory of neuronal branching and its practical application. PLoS Comput. Biol. *6*, 6.

Feinberg, E.H., Vanhoven, M.K., Bendesky, A., Wang, G., Fetter, R.D., Shen, K., and Bargmann, C.I. (2008). GFP Reconstitution Across Synaptic Partners (GRASP) defines cell contacts and synapses in living nervous systems. Neuron *57*, 353–363.

Fischbach, K.F., and Dittrich, A.P. (1989). The optic lobe of *Drosophila melanogaster*. I. A Golgi analysis of wild-type structure. Cell Tissue Res. *258*, 441–475.

Fischer, R.S., Wu, Y., Kanchanawong, P., Shroff, H., and Waterman, C.M. (2011). Microscopy in 3D: a biologist's toolbox. Trends Cell Biol. *21*, 682–691.

Gao, S., Takemura, S.Y., Ting, C.Y., Huang, S., Lu, Z., Luan, H., Rister, J., Thum, A.S., Yang, M., Hong, S.T., et al. (2008). The neural substrate of spectral preference in *Drosophila*. Neuron *60*, 328–342.

Gesualdi, S.C., and Haerry, T.E. (2007). Distinct signaling of *Drosophila* Activin/TGF-beta family members. Fly (Austin) *1*, 212–221.

Gordon, M.D., and Scott, K. (2009). Motor control in a *Drosophila* taste circuit. Neuron *61*, 373–384.

Han, C., Wang, D., Soba, P., Zhu, S., Lin, X., Jan, L.Y., and Jan, Y.N. (2012). Integrins regulate repulsion-mediated dendritic patterning of *drosophila* sensory neurons by restricting dendrites in a 2D space. Neuron *73*, 64–78.

Huang, Z., and Kunes, S. (1996). Hedgehog, transmitted along retinal axons, triggers neurogenesis in the developing visual centers of the *Drosophila* brain. Cell *86*, 411–422.

Huang, Z., Shilo, B.Z., and Kunes, S. (1998). A retinal axon fascicle uses spitz, an EGF receptor ligand, to construct a synaptic cartridge in the brain of *Drosophila*. Cell *95*, 693–703.

Jan, Y.N., and Jan, L.Y. (2010). Branching out: mechanisms of dendritic arborization. Nat. Rev. Neurosci. *11*, 316–328.

Jarman, A.P., Grell, E.H., Ackerman, L., Jan, L.Y., and Jan, Y.N. (1994). Atonal is the proneural gene for *Drosophila* photoreceptors. Nature *369*, 398–400.

Kaplan, E.L., and Meier, P. (1958). Nonparametric Estimation from Incomplete Observations. J. Am. Stat. Assoc. *53*, 457–481.

Kunes, S., and Steller, H. (1991). Ablation of *Drosophila* photoreceptor cells by conditional expression of a toxin gene. Genes Dev. *5*, 970–983.

Lee, T., and Luo, L. (1999). Mosaic analysis with a repressible cell marker for studies of gene function in neuronal morphogenesis. Neuron *22*, 451–461.

Lee, T., Winter, C., Marticke, S.S., Lee, A., and Luo, L. (2000). Essential roles of *Drosophila* RhoA in the regulation of neuroblast proliferation and dendritic but not axonal morphogenesis. Neuron *25*, 307–316.

Lefebvre, J.L., Kostadinov, D., Chen, W.V., Maniatis, T., and Sanes, J.R. (2012). Protocadherins mediate dendritic self-avoidance in the mammalian nervous system. Nature *488*, 517–521.

Li, X., Erclik, T., Bertet, C., Chen, Z., Voutev, R., Venkatesh, S., Morante, J., Celik, A., and Desplan, C. (2013). Temporal patterning of *Drosophila* medulla neuroblasts controls neural fates. Nature *498*, 456–462.

London, M., and Häusser, M. (2005). Dendritic computation. Annu. Rev. Neurosci. *28*, 503–532.

Luan, H., Peabody, N.C., Vinson, C.R., and White, B.H. (2006). Refined spatial manipulation of neuronal function by combinatorial restriction of transgene expression. Neuron *52*, 425–436.

Masland, R.H. (2012). The neuronal organization of the retina. Neuron *76*, 266–280.

Matsuoka, R.L., Nguyen-Ba-Charvet, K.T., Parray, A., Badea, T.C., Chédotal, A., and Kolodkin, A.L. (2011). Transmembrane semaphorin signalling controls laminar stratification in the mammalian retina. Nature *470*, 259–263.

Matthews, B.J., Kim, M.E., Flanagan, J.J., Hattori, D., Clemens, J.C., Zipursky, S.L., and Grueber, W.B. (2007). Dendrite self-avoidance is controlled by Dscam. Cell *129*, 593–604.

Melnattur, K.V., and Lee, C.H. (2011). Visual circuit assembly in *Drosophila*. Dev. Neurobiol. *71*, 1286–1296.

Ng, J. (2008). TGF-beta signals regulate axonal development through distinct Smad-independent mechanisms. Development *135*, 4025–4035.

O'Connor, M.B., Umulis, D., Othmer, H.G., and Blair, S.S. (2006). Shaping BMP morphogen gradients in the *Drosophila* embryo and pupal wing. Development *133*, 183–193.

Parker, L., Ellis, J.E., Nguyen, M.Q., and Arora, K. (2006). The divergent TGF-beta ligand Dawdle utilizes an activin pathway to influence axon guidance in *Drosophila*. Development *133*, 4981–4991.

Pecot, M.Y., Tadros, W., Nern, A., Bader, M., Chen, Y., and Zipursky, S.L. (2013). Multiple interactions control synaptic layer specificity in the *Drosophila* visual system. Neuron *77*, 299–310.

Sanes, J.R., and Zipursky, S.L. (2010). Design principles of insect and vertebrate visual systems. Neuron *66*, 15–36.

Scorcioni, R., Polavaram, S., and Ascoli, G.A. (2008). L-Measure: a web-accessible tool for the analysis, comparison and search of digital reconstructions of neuronal morphologies. Nat. Protoc. *3*, 866–876.

Takemura, S.Y., Lu, Z., and Meinertzhagen, I.A. (2008). Synaptic circuits of the *Drosophila* optic lobe: the input terminals to the medulla. J. Comp. Neurol. *509*, 493–513.

Takemura, S.Y., Karuppudurai, T., Ting, C.Y., Lu, Z., Lee, C.H., and Meinertzhagen, I.A. (2011). Cholinergic circuits integrate neighboring visual signals in a *Drosophila* motion detection pathway. Curr. Biol. *21*, 2077–2084.

Takemura, S.Y., Bharioke, A., Lu, Z., Nern, A., Vitaladevuni, S., Rivlin, P.K., Katz, W.T., Olbris, D.J., Plaza, S.M., Winston, P., et al. (2013). A visual motion detection circuit suggested by *Drosophila* connectomics. Nature *500*, 175–181.

Timofeev, K., Joly, W., Hadjieconomou, D., and Salecker, I. (2012). Localized netrins act as positional cues to control layer-specific targeting of photoreceptor axons in *Drosophila*. Neuron *75*, 80–93.

Ting, C.Y., Yonekura, S., Chung, P., Hsu, S.N., Robertson, H.M., Chiba, A., and Lee, C.H. (2005). *Drosophila* N-cadherin functions in the first stage of the two-stage layer-selection process of R7 photoreceptor afferents. Development *132*, 953–963.

Ting, C.Y., Herman, T., Yonekura, S., Gao, S., Wang, J., Serpe, M., O'Connor, M.B., Zipursky, S.L., and Lee, C.H. (2007). Tiling of r7 axons in the *Drosophila* visual system is mediated both by transduction of an activin signal to the nucleus and by mutual repulsion. Neuron *56*, 793–806.

Tomasi, T., Hakeda-Suzuki, S., Ohler, S., Schleiffer, A., and Suzuki, T. (2008). The transmembrane protein Golden goal regulates R8 photoreceptor axon-axon and axon-target interactions. Neuron *57*, 691–704.

Völgyi, B., Chheda, S., and Bloomfield, S.A. (2009). Tracer coupling patterns of the ganglion cell subtypes in the mouse retina. J. Comp. Neurol. *512*, 664–687.

Wen, Q., Stepanyants, A., Elston, G.N., Grosberg, A.Y., and Chklovskii, D.B. (2009). Maximization of the connectivity repertoire as a statistical principle governing the shapes of dendritic arbors. Proc. Natl. Acad. Sci. USA *106*, 12536–12541.

Wong, A.M., Wang, J.W., and Axel, R. (2002). Spatial representation of the glomerular map in the *Drosophila* protocerebrum. Cell *109*, 229–241.

Yamagata, M., and Sanes, J.R. (2008). Dscam and Sidekick proteins direct lamina-specific synaptic connections in vertebrate retina. Nature *451*, 465–469.

Zheng, X., Wang, J., Haerry, T.E., Wu, A.Y., Martin, J., O'Connor, M.B., Lee, C.H., and Lee, T. (2003). TGF-beta signaling activates steroid hormone receptor expression during neuronal remodeling in the *Drosophila* brain. Cell *112*, 303–315.